NAVAL POSTGRADUATE SCHOOL
Monterey, California

THESIS

EXAMINATION OF TIME-REVERSAL ACOUSTIC APPLICATIONS TO SHALLOW WATER ACTIVE SONAR SYSTEMS

by

Thomas A. Winter

March 2000

Thesis Advisor:	Kevin B. Smith
Second Reader:	Mitch Shipley

Approved for public release; distribution is unlimited.

DTIC QUALITY INSPECTED 4

20000623 100

REPORT DOCUMENTATION PAGE

Form Approved OMB No. 0704-0188

Public reporting burden for this collection of information is estimated to average 1 hour per response, including the time for reviewing instruction, searching existing data sources, gathering and maintaining the data needed, and completing and reviewing the collection of information. Send comments regarding this burden estimate or any other aspect of this collection of information, including suggestions for reducing this burden, to Washington headquarters Services, Directorate for Information Operations and Reports, 1215 Jefferson Davis Highway, Suite 1204, Arlington, VA 22202-4302, and to the Office of Management and Budget, Paperwork Reduction Project (0704-0188) Washington DC 20503.

1. AGENCY USE ONLY *(Leave blank)*	2. REPORT DATE	3. REPORT TYPE AND DATES COVERED
	March 2000	Master's Thesis

4. TITLE AND SUBTITLE
Examination of Time-Reversal Acoustic Applications to Shallow Water Active Sonar Systems

5. FUNDING NUMBERS

6. AUTHOR(S)
Winter, Thomas A.

7. PERFORMING ORGANIZATION NAME(S) AND ADDRESS(ES)
Naval Postgraduate School
Monterey, CA 93943-5000

8. PERFORMING ORGANIZATION REPORT NUMBER

9. SPONSORING / MONITORING AGENCY NAME(S) AND ADDRESS(ES)

10. SPONSORING / MONITORING AGENCY REPORT NUMBER

11. SUPPLEMENTARY NOTES
The views expressed in this thesis are those of the author and do not reflect the official policy or position of the Department of Defense or the U.S. Government.

12a. DISTRIBUTION / AVAILABILITY STATEMENT
Approved for public release; distribution unlimited.

12b. DISTRIBUTION CODE

13. ABSTRACT *(maximum 200 words)*

The ability to employ effectively an active sonar system in the littoral regions is of great interest to the United States Navy. Time-varying multipath propagation introduces significant problems that must be overcome in the employment of shallow water active sonar. The phenomenon of time-reversal acoustics (TRA) has provided hope for a solution to this problem by undoing much of the multipath spreading without the need to have knowledge of the environment in these littoral regions. When an active sonar return is time-reversed (phase-conjugated in the frequency domain) and retransmitted, this second signal focuses in time and space back at the original source location. This thesis investigates the phenomenon of TRA as it applies to an idealized shallow water environment. Numerical modeling was performed for a variety of source and target apertures and ranges. Results demonstrate a significant enhancement in received active sonar signal strength due to the TRA acoustic field focusing effect. Furthermore, the signal strength enhancement remains significant even when the source to target range changes between active sonar transmissions. The results presented in this thesis demonstrate that the use of TRA may provide substantial signal to noise ratio improvements over current active sonar systems. Further modeling and real world experiments could ultimately lead to the development of a practical active TRA sonar system.

14. SUBJECT TERMS	15. NUMBER OF PAGES
Time-reversal, acoustics, active sonar	73
	16. PRICE CODE

17. SECURITY CLASSIFICATION OF REPORT	18. SECURITY CLASSIFICATION OF THIS PAGE	19. SECURITY CLASSIFI- CATION OF ABSTRACT	20. LIMITATION OF ABSTRACT
Unclassified	Unclassified	Unclassified	Unlimited

Approved for public release; distribution is unlimited

EXAMINATION OF TIME-REVERSAL ACOUSTIC APPLICATIONS TO SHALLOW WATER ACTIVE SONAR SYSTEMS

Thomas A. Winter
Lieutenant, United States Navy
B.S., University of Notre Dame, 1993

Submitted in partial fulfillment of the
requirements for the degree of

MASTER OF SCIENCE IN ENGINEERING ACOUSTICS

from the

NAVAL POSTGRADUATE SCHOOL
March 2000

Author: 

Thomas A. Winter

Approved by: 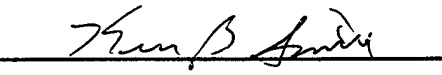

Kevin B. Smith, Thesis Advisor

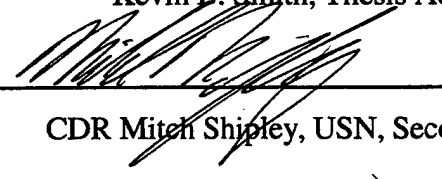

CDR Mitch Shipley, USN, Second Reader

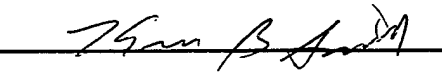

Kevin B. Smith, Chairman, Engineering
Acoustics Academic Committee

ABSTRACT

The ability to employ effectively an active sonar system in the littoral regions is of great interest to the United States Navy. Time-varying multipath propagation introduces significant problems that must be overcome in the employment of shallow water active sonar. The phenomenon of time-reversal acoustics (TRA) has provided hope for a solution to this problem by undoing much of the multipath spreading without the need to have knowledge of the environment in these littoral regions. When an active sonar return is time-reversed (phase-conjugated in the frequency domain) and retransmitted, this second signal focuses in time and space back at the original source location.

This thesis investigates the phenomenon of TRA as it applies to an idealized shallow water environment. Numerical modeling was performed for a variety of source and target apertures and ranges. Results demonstrate a significant enhancement in received active sonar signal strength due to the TRA acoustic field focusing effect. Furthermore, the signal strength enhancement remains significant even when the source to target range changes between active sonar transmissions.

The results presented in this thesis demonstrate that the use of TRA may provide substantial signal to noise ratio improvements over current active sonar systems. Further modeling and real world experiments could ultimately lead to the development of a practical active TRA sonar system.

TABLE OF CONTENTS

I. INTRODUCTION

The United States Navy has in recent years focused its attention on the shallow water littoral regions of the world's oceans. These regions present a multitude of problems in the effort to effectively employ active sonar systems. Time-varying multipath propagation is one of the more significant problems encountered. It has been shown that the acoustic phenomenon of time reversal can minimize this problem in applications relating to underwater communication (Abrantes, 1999 and Smith et al, 2000). This has provided hope that time-reversal acoustics could improve the effectiveness of active sonar systems in these shallow water regions. This thesis studies the effects of time-reversal acoustics as it relates to active sonar system applications.

In order to study the applicability of time-reversal acoustics to an active sonar system, both computer modeling and experimental work are required. This thesis exclusively uses computer modeling to study the time-reversal phenomenon. Various scenarios were simulated using a very accurate and highly computationally intensive acoustic propagation model. These scenarios all involved determining the signal return from an active sonar transmission that reflected off a target. The scenarios differed in target range, target size, target movement, and source/receiver aperture.

The measure of effectiveness used in this thesis to determine the advantages of time-reversal methods was minimum pulse transmission loss. A comparison was made between the minimum pulse transmission losses for a single pulse return from a target and for a time-reversed transmission return from the same target. While other measures of effectiveness could reasonably be used, this one provides a real sense of the improvement in signal strength due to time-reversal methods.

This thesis is presented in five chapters. This introduction has laid out the basic problem that the remainder of the thesis will attempt to address. The second chapter lays the groundwork for the theory behind time-reversal acoustics. It first explains the time-reversal phenomenon in a visually intuitive manner, and then rigorously derives the underlying mathematical equations that govern time-reversal acoustics. The third chapter introduces the acoustic propagation model used for this work, the Monterey-Miami Parabolic Equation (MMPE) model. The parabolic equation is derived starting from the Helmholtz equation, and the concept of reciprocity is introduced. Methods for solving and implementing the parabolic equation are then presented. Finally, a description of the MMPE model including its inputs and outputs is given. The fourth chapter presents the results obtained from the simulations run for this thesis. This chapter compares the time arrival structures of a pulse reflected off a target and a time-reversed transmission return off the same target. Results are presented for various aperture sizes, target ranges, and for stationary targets as well as

targets which have moved. The final chapter offers conclusions based on the results given in Chapter Four. The argument will be made that a sonar system that employs time-reversal acoustic methods can enjoy significant advantages over conventional sonar systems.

THIS PAGE INTENTIONALLY LEFT BLANK

II. THEORY OF TIME REVERSAL ACOUSTICS

This chapter will present the theory behind the development of a time reversal acoustics (TRA) system. The theoretical development will be presented in two sections. The first will provide a visual understanding of the process of time reversal acoustics. Using the notion of the ocean as a black box filter, this section will show how the ocean can be used as an autocorrelator without knowing the details of the ocean environment. In the second section, the mathematical foundations of TRA will be presented, starting from the principles of the Helmholtz equation and reciprocity.

A. VISUAL DEMONSTRATION OF TRA

To visualize the process of time reversal acoustics, consider the following ocean environment with the propagation paths as shown in Figure 2.1. In this simple example considering only point sources and receivers, there are only

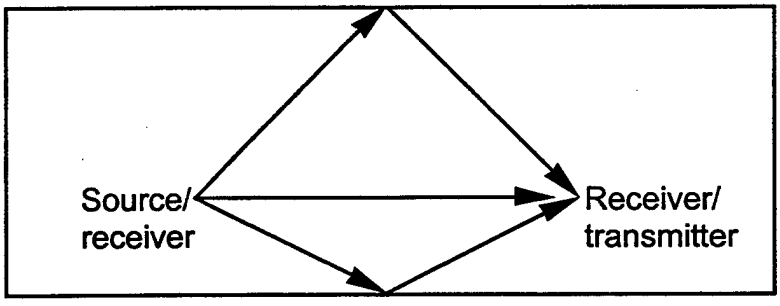

Figure 2.1

three propagation paths between source and receiver/transmitter. A pulse transmitted from the source at arbitrary time t_0 will arrive at the receiver at three distinct times, due to the three different propagation path lengths. This is shown in Figure 2.2. At the receiver, the signal is recorded and reversed in time. This

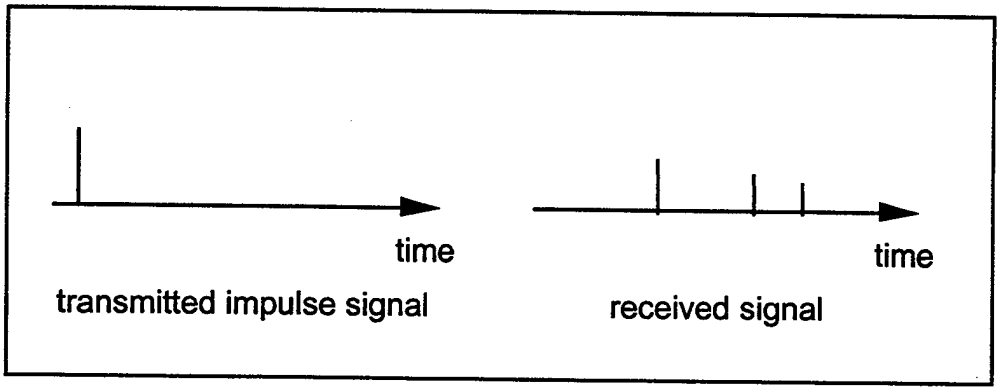

Figure 2.2

time-reversed signal is then transmitted from the receiver/transmitter back into the ocean. The retransmitted signal consists of three distinct impulses corresponding to the three arrivals at the receiver. Each of these impulses propagates back toward the original source along the three possible propagation paths. Thus, a total of nine impulses are received back at the original source. Three of these nine impulses will arrive at exactly the same time- the three impulses that traveled back along the path that corresponds to the path the signal traveled when it was first received. The three impulses that arrive at the same time combine to form a pressure peak that is significantly higher than the originally received signal. The other six impulses are also detected back at the

original source, and appear as sidelobes next to the higher peak pressure as shown in Figure 2.3.

Another important factor to note is that the retransmitted signal amplitude was assumed to have been normalized back to the maximum amplitude available from the source. Thus the SNR gain realized after TRA is a product of two factors, the signal amplitude addition due to the combination of received signals

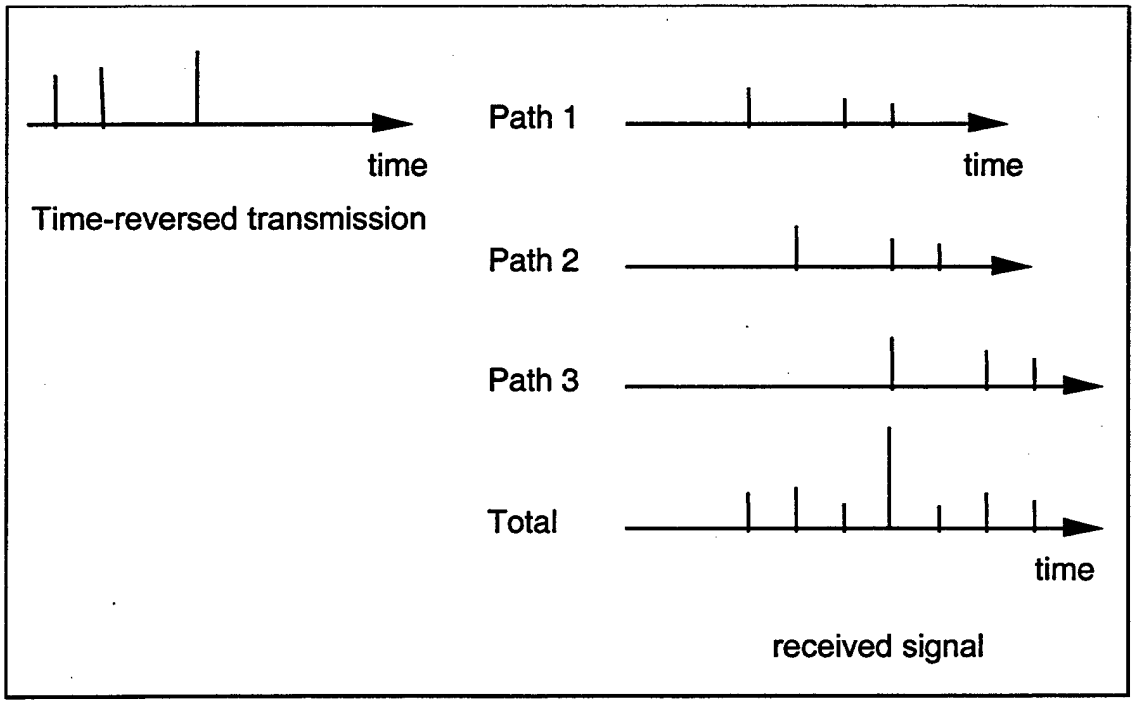

Figure 2.3

from various multipath propagations and the increase in energy in the retransmitted signal. Only the highest pressure peak received was normalized back to the maximum amplitude available from the source; all others were scaled proportionally. The difference in magnitudes of the received impulses results

from the difference in spreading, absorption, and boundary interaction losses suffered in the various paths.

B. MATHEMATICAL DERIVATION

For use in the mathematical derivation, consider the ideal waveguide shown in Figure 2.4. This waveguide has a pressure release surface and a rigid bottom. The coordinate system is as shown, with the horizontal axis from o to o' being the reference axis for propagation, and the vertical axes z and z_S measured positive in the downward direction. The relationship among the coordinates is given by $z' = z$ and $r' = R - r$.

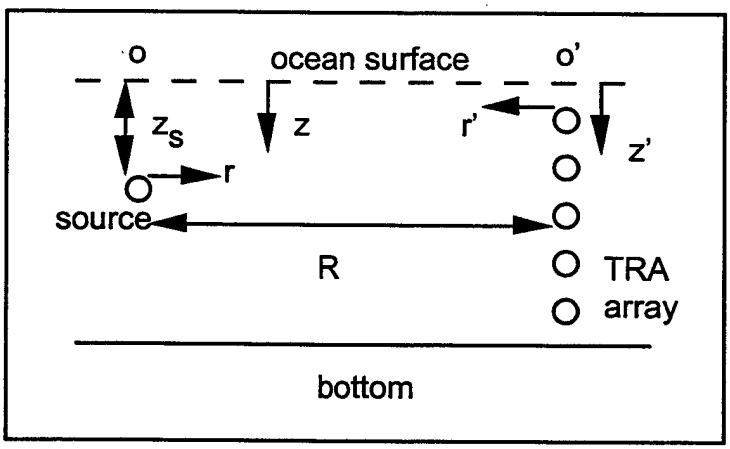

Figure 2.4

The foundation for the theoretical development of time reversal acoustics (TRA) comes from two important sources, the Helmholtz equation and the

principle of reciprocity. The Helmholtz equation, or frequency domain wave equation, is given by

$$[\nabla^2 + k^2(z)]G(r,z \mid z_S,\omega) = -\delta(r)\delta(z - z_S) \tag{2.1}$$

where $k(z) = \frac{\omega}{c(z)}$ is the acoustic wavenumber for a waveguide with sound speed c(z), $\omega = 2\pi f$ is the angular frequency corresponding to the acoustic frequency f, and $G(r,z \mid z_s,\omega)$ is the frequency dependent Green's function at location (r,z) due to a source at $(r = 0, z = z_s)$. This Green's function can be interpreted as a representation of an impulse response produced by a point source at range $r = 0$ and depth $z = z_s$, measured by a point receiver at range r and depth z. From this, it has been shown (Jensen et al., 1994) that the Green's function satisfies the principle of reciprocity given by

$$\rho(\vec{r}_s)G(\vec{r}_j \mid \vec{r}_s,\omega) = \rho(\vec{r}_j)G(\vec{r}_s \mid \vec{r}_j,\omega). \tag{2.2}$$

In words, the acoustic field function measured at a given point $\vec{r}_j$ due to a point source located at point $\vec{r}_s$ is the same as the acoustic field function measured at $\vec{r}_s$ due to a point source located at $\vec{r}_j$, scaled by the densities of the medium at $\vec{r}_s$ and $\vec{r}_j$. For purposes of this development, the medium is homogenous and this leads to reciprocity of the acoustic field function alone,

$$G(\vec{r}_j \mid \vec{r}_s, \omega) = G(\vec{r}_s \mid \vec{r}_j, \omega). \tag{2.3}$$

This is an extremely important result that is critical to TRA. The acoustic signal that arrives at a given array element has been modified by the environment between source and receiver; essentially, the environment acts as a transfer function. When each element of the array then transmits back the time reversed signal, the signal is modified in a reciprocal way and the signal received at the original source no longer contains the effects of the environment. Because of reciprocity, the effect of environment on the structure of the received signal is greatly reduced. It should be noted that this is true only if the environment is static. If the environment changes between transmissions the transfer functions will not be matched, and the received signal will not be identical to the original signal. The difference between transmitted and received signals will be related to the amount of change in the environment between transmissions. For relatively minor changes, which are expected over short time periods in an ocean environment, the difference between transmitted and received signals is expected to be relatively small.

A good illustration of this principle is the effect of multipath propagation. Consider a point source and a vertical array some distance away, as shown in Figure 2.5. The signal received at the array has multiple arrivals due to the many

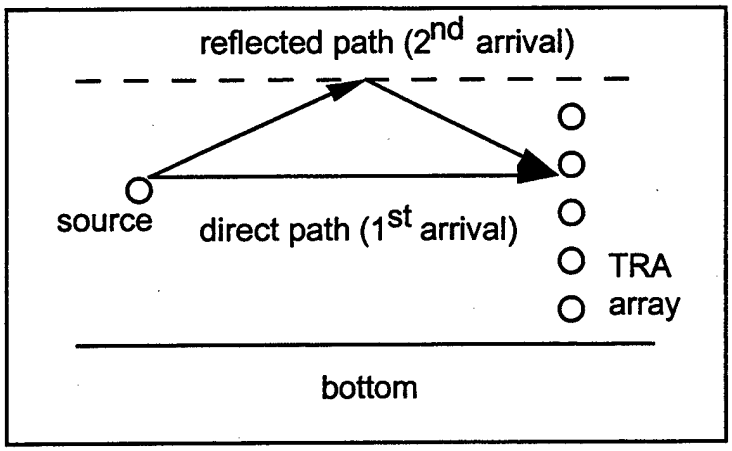

Figure 2.5

paths the signal can take. The direct path signal arrives first, followed by other, longer paths. For simplicity, Figure 2.5 shows only two paths. After the signal is received at the array it is time-reversed and retransmitted. This transmission is done in the reverse order of the received signal. In other words the reflected path signal, which was received last, is now transmitted first. The direct path signal is transmitted last, after a delay equal to the delay between the reception of the original signals. The result is a matched filter of the original signal back at the original source. It is important to realize that there will be sidelobes present at the original source due to the multipath propagation of the time-reversed signal.

In order to solve the Helmholtz wave equation, the method of separation of variables may be used (Jensen et al., 1994). The solution to the Helmholtz

equation is given in terms of normal modes, or eigenfunctions, which are depth-dependent, and Hankel functions, which are range dependent. The far field approximation to the solution is given by

$$G(r,z\,|\,z_S,\omega)=\frac{i}{\rho(z_S)\sqrt{8\pi r}}e^{-i\frac{\pi}{4}}\sum_{m=1}^{\infty}\Psi_m(z_S)\Psi_m(z)\frac{e^{iK_m r}}{\sqrt{K_m}} \tag{2.4}$$

where $G(r,z\,|\,z_S,\omega)$ is the pressure field at the point (r,z) due to a point source at z_S adjusted so that the pressure at range $r=1m$ is unity, r is the horizontal distance from the source, $\Psi_m(z)$ is the normal mode eigenfunction, and K_m is the modal wavenumber. The normal mode eigenfunction $\Psi_m(z)$ and modal wavenumber K_m are found by solving this eigenvalue problem which has known boundary conditions

$$\frac{d^2\Psi_m(z)}{dz^2}+[k^2(z)-K_m^2]\Psi_m(z)=0\,. \tag{2.5}$$

The normal mode eigenfunctions form a complete set, expressed as

$$\Sigma\frac{\Psi_m(z)\Psi_m(z_S)}{\rho(z_S)}=\delta(z-z_S) \tag{2.6}$$

and satisfy the orthonormality condition, expressed as

$$\int_0^{\infty}\frac{\Psi_m(z)\Psi_n(z_S)}{\rho(z_S)}dz=\delta_{mn}. \tag{2.7}$$

With the Helmholtz equation thus solved, the signal received at the array for a given source transmission $s(t)$ can be expressed as (Kuperman et al., 1998)

$$p(R,z_j,t) = \int G(R,z_j \mid z_S,\omega)S(\omega)e^{-i\omega t}d\omega \qquad (2.8)$$

where $S(\omega)$ is the Fourier transform of $s(t)$. This is the signal that must be time-reversed.

At this point it should be noted that time reversal in the time domain is equivalent to phase conjugation in the frequency domain. This is due to the time-reversal property of the Fourier transform. Assuming a signal $s(t)$ is real,

$$\mathbf{F}[s(t)] = S(\omega) \qquad (2.9)$$

then

$$\mathbf{F}[s(-t)] = S(-\omega) = S^*(\omega). \qquad (2.10)$$

Thus, time reversal is accomplished by a phase conjugation of the signal in the frequency domain.

When the signal received at the array, as expressed by equation (2.8), is time-reversed it becomes

$$p(R,z_j,T-t) = \int_{-\infty}^{\infty} G(R,z_j \mid z_j,\omega)S(\omega)e^{-i\omega(T-t)}d\omega. \qquad (2.11)$$

This assumes that the received signal is confined to a time period $(0,\tau)$, and $T > 2\tau$. This is necessary to ensure causality. If $T < 2\tau$, the signal would in effect be reversed *before* it was received. Going one step further, the time-reversed signal can be written

$$p(R,z_j,T-t) = \int_{\infty}^{-\infty} G(r,z_j \mid z_j,-\omega)S(-\omega)e^{i\omega T}e^{-i\omega t}(-d\omega) \qquad (2.12)$$

or

$$p(R,z_j,T-t)=\int_{-\infty}^{\infty}[G^*(r,z_j\,|\,z_j,\omega)S^*(-\omega)e^{i\omega T}]e^{-i\omega t}d\omega. \qquad (2.13)$$

Now that the signal transmitted by the array back toward the source has been determined, the acoustic field generated by the array can be calculated. The total field is a summation of the field due to each element of the array. Since $G(r',z\,|\,z_j,\omega)$ is the acoustic field at the location (r',z) due to a point source at the element j, the acoustic field due to the time-reversed signal from element j is given by

$$P(r',z\,|\,z_j,\omega)=G(r',z\,|\,z_j,\omega)G^*(R,z_j\,|\,z_S,\omega)S^*(\omega)e^{i\omega T}. \qquad (2.14)$$

Summing over all elements, the acoustic field due to the time-reversed signal from the array is given by

$$P(r',z\,|\,\omega)=\sum_j G(r',z\,|\,z_j,\omega)G^*(R,z_j\,|\,z_S,\omega)S^*(\omega)e^{i\omega T}. \qquad (2.15)$$

In the time domain the signal is expressed as

$$P(r',z,t)=\sum_j\int G(r',z\,|\,z_j,\omega)G^*(R,z_j\,|\,z_S,\omega)S^*(\omega)e^{i\omega T}e^{-i\omega t}d\omega. \qquad (2.16)$$

Employing the principle of reciprocity as expressed in equation (2.3), the time domain signal back at the original source is then given by (Kuperman et al., 1998)

$$P(R,z_S,t)=\frac{1}{(2\pi)^2}\int\{\sum_j[\int g_{t'+t''}(R,z_S\,|\,z_j,\omega)g_{t'}(R,z_S\,|\,z_j,\omega)dt']\times s(t''-t+T)\}dt'' \qquad (2.17)$$

where $g_{t'+t''}(R,z_S \mid z_j,\omega), g_{t'}(R,z_S \mid z_j,\omega)$ and $s(t''-t+T)$ are the time domain representations of the Green's function and the original signal. The effect of time-reversal acoustics is seen in equation (2.17); the Green's function is correlated with itself! As pointed out by Kuperman et al., 1994, this is a form of matched filtering, with the filter matched to the transfer function of the ocean from the source to each element in the array. This matched filtering provides a temporal focusing effect.

The time-reversal transmission of the array also produces a spatial focusing effect. The acoustic field due to the time-reversed field from the array is given by equation (2.15). Equation (2.17) provides the far field approximation to the Helmholtz equation. Combining these two equations yields

$$P(r',z,\omega)=\frac{S^*(\omega)e^{i\omega T}}{\rho(z_S)8\pi\sqrt{Rr'}}\sum_j\sum_m\sum_n\frac{\Psi_m(z)\Psi_m(z_j)\Psi_n(z_S)\Psi_n(z_j)}{\rho(z_j)\sqrt{K_mK_n}}e^{i(K_mr'-K_nR)}. \quad (2.18)$$

If the assumption is made that the array has sufficient elements to adequately sample all modes, then the summation over j in equation (2.18) can be approximated by an integral, and equation (2.18) becomes

$$P(r',z,\omega)\approx S^*(\omega)e^{i\omega T}\sum_m\sum_n\frac{\Psi_m(z)\Psi_n(z_S)e^{i(K_mr'-K_nR)}}{\rho(z_S)8\pi\sqrt{Rr'}\sqrt{K_mK_n}}\int_0^\infty\frac{\Psi_m(z)\Psi_n(z)}{\rho(z)}dz. \quad (2.19)$$

Applying the orthogonality property of the normal modes and evaluating at the source range $(r'=R)$ gives

$$P(R,z,\omega)\approx S^*(\omega)e^{i\omega T}\sum_m\frac{\Psi_m(z)\Psi_m(z_S)}{\rho(z_S)8\pi RK_m}. \quad (2.20)$$

Using the fact that the normal modes form a complete set, as expressed by equation (2.6), and the assumption that K_m is essentially constant over the contributing modes leads to

$$P(R,z,\omega) \approx \frac{S^*(\omega)e^{i\omega T}}{8\pi RK} \sum_m \frac{\Psi_m(z)\Psi_m(z_S)}{\rho(z_S)} \tag{2.21}$$

and

$$P(R,z,\omega) \approx \frac{S^*(\omega)e^{i\omega T}}{8\pi RK} \delta(z - z_S). \tag{2.22}$$

The delta function on the right hand side of this equation shows clearly the vertical focusing effect at the source range. One important assumption used in the derivation of equation (2.22) is the closure property of the modes, which requires all modes to be adequately sampled by the array. For arrays with small apertures this focusing effect will not be as pronounced. Abrantes (1999) showed that a good quality of focus could be achieved even with relatively small aperture arrays. This thesis will expand upon the work of Abrantes (1999) and attempt to determine the quality of the focusing effect in an active sonar system applicable to submarine use.

III. NUMERICAL MODELING METHODS EMPLOYED

This chapter provides a background understanding of the principles involved in modeling acoustic propagation using a parabolic approximation to the wave equation, and a description of the model actually used in this thesis, the Monterey-Miami Parabolic Equation (MMPE). This information will be presented in four sections. The first section will derive the form of the wave equation used by the MMPE propagation model, and explain in mathematical terms the physics behind the parabolic approximation. Next, the method of implementation of the parabolic approximation, known as the split-step Fourier (SSF) algorithm, is described. In the third section, the details of input and output of the MMPE are shown. Finally, the last section explains how the MMPE calculates the time arrival structure of a signal. It is this time arrival structure which will constitute the majority of the data presented in the next chapter.

A. PARABOLIC APPROXIMATION TO THE WAVE EQUATION

Tappert (1974) first introduced the general form of the parabolic approximation to the wave equation that is employed in the MMPE. In order to arrive at this approximation, let the time-harmonic acoustic field be represented by

$$P(r,z,\phi,\omega t) = p(r,z,\phi)e^{-i\omega t} \tag{3.1}$$

in cylindrical coordinates. The use of cylindrical coordinates is especially useful in shallow water acoustics since the acoustic propagation is primarily horizontal with limited vertical propagation. Substituting Equation (3.1) into the wave equation produces a cylindrical coordinate version of Equation (2.1),

$$\frac{1}{r}\frac{\partial}{\partial r}(r\frac{\partial p}{\partial r})+\frac{1}{r^2}\frac{\partial^2 p}{\partial \phi^2}+\frac{\partial^2 p}{\partial z^2}+k_0^2 n^2(r,z,\phi)p=-4\pi P_0\delta(\vec{x}-\vec{x}_S) \qquad (3.2)$$

where $k_0=\frac{\omega}{c_0}$ is the reference wavenumber, $n(r,z,\phi)=\frac{c_0}{c(r,z,\phi)}$ is the acoustic index of refraction, c_0 is the reference sound speed, and $c(r,z,\phi)$ is the acoustic sound speed. This right hand side of this form of the Helmholtz equation is the source function, a point source at location $(r=0,z=z_S)$. This point source has a reference level P_0, which is defined as the pressure amplitude at a reference distance of 1 m. The environment is incorporated into the equation through the $c(r,z,\phi)$ term.

This form of the Helmholtz equation can be simplified by defining

$$p(r,z)=\frac{1}{\sqrt{r}}u(r,z). \qquad (3.3)$$

This term accounts for the cylindrical spreading that dominates the propagation, and when substituted into the Helmholtz equation yields

$$\frac{\partial^2 u}{\partial r^2}+\frac{1}{r^2}\frac{\partial^2 u}{\partial \phi^2}+\frac{\partial^2 u}{\partial z^2}+k_0^2(n^2+\frac{1}{4k_0^2r^2})u=0. \qquad (3.4)$$

The final term in Equation (3.4) is neglected since it drops off as $1/r^2$. The second term in Equation (3.4) affects the azimuthal coupling between radials. This term is generally small and is ignored to arrive at the uncoupled azimuth approximation.

With the final term of Equation (3.4) ignored, the resulting Helmholtz equation can be factored by introducing the operator

$$P_{op} = \frac{\partial}{\partial r} \tag{3.5}$$

and

$$Q_{op} = (\mu + \varepsilon + 1)^{1/2}, \tag{3.6}$$

where

$$\varepsilon = n^2 - 1 \text{ and } \mu = \frac{1}{k_0^2}\frac{\partial^2}{\partial z^2}. \tag{3.7}$$

Then the homogeneous form of the Helmholtz equation (3.2) becomes

$$(P_{op}^2 + k_0^2 Q_{op}^2)u = 0. \tag{3.8}$$

The outward propagating field can be factored by defining

$$u = Q_{op}^{-1/2}\Psi. \tag{3.9}$$

The Q_{op} factor is included to ensure the proper initial condition of the starting field and for power conservation. It is also assumed that there is weak range

dependence in the environment, and thus the commutator $[P_{op}, Q_{op}]$ is negligible. With these conditions, the outgoing wave satisfies

$$P_{op}\Psi = ik_0 Q_{op}\Psi \tag{3.10}$$

or

$$-ik_0^{-1}\frac{\partial \Psi}{\partial r} = Q_{op}\Psi. \tag{3.11}$$

Equation (3.11) completely describes the forward propagating acoustic energy in the waveguide when backscattered energy is considered negligible. This is the parabolic form of the acoustic wave equation, and it is the starting point for all PE acoustic models including the MMPE. The difference between PE models lies in the method of solving this equation. Ultimately, the differences result from the development of various approximations to the pseudo-differential operator Q_{op}.

B. NUMERICAL SOLUTION

The method of solution employed by the MMPE recognizes the fact that the acoustic field can be decomposed into two terms. The first is a slowly modulating envelope function, and the second is a phase term that oscillates at the acoustic frequency. The envelope function is also called the PE field function $\psi(r, z, \phi)$, and is defined as

$$\Psi = \psi e^{ik_0 r} \tag{3.12}$$

or

$$p(r,z,\phi) = P_0\sqrt{\frac{R_0}{r}}Q_{op}^{-1/2}\psi(r,z,\phi)e^{ik_0 r}. \tag{3.13}$$

This definition of the PE field function is scaled such that at $r = R_0$, $|\psi| = 1$ and $|p| = P_0$.

When this expression is substituted into the Helmholtz equation it produces

$$\frac{\partial\psi}{\partial r} = -ik_0\psi + ik_0 Q_{op}\psi = -ik_0 H_{op}\psi, \tag{3.14}$$

where

$$H_{op} = 1 - Q_{op} = T_{op} + U_{op} \tag{3.15}$$

is a Hamiltonian-like operator that defines the evolution of the PE field function in range. The operators on the right side of Equation (3.15) are defined as

$$T_{op} = -\frac{1}{k_0^2}\frac{\partial^2}{\partial z^2}[(1+\frac{1}{k_0^2}\frac{\partial^2}{\partial z^2})+1]^{-1} \tag{3.16}$$

and

$$U_{op} = -(n-1), \tag{3.17}$$

introduced by Thomson and Chapman (1983). This approximation is known as the wide-angle parabolic equation (WAPE) approximation. This approximation has proven highly accurate for angles of propagation up to 40 to 70 degrees, depending on environment type (Chin-Bing et al., 1993).

In solving the WAPE approximation to the parabolic equation, the MMPE model uses a split-step Fourier (SSF) algorithm (Hardin and Tappert, 1973).

Because the parabolic equation method utilizes a first order differential equation version of the wave equation, the SSF algorithm can implement a non-iterative marching solution method. This method applies the U_{op} operator in the z-domain and the T_{op} operator in the k_z-domain in order to integrate the solution in range. These operators are defined in their respective domains as

$$U_{op}(z) = -[n(z) - 1] \tag{3.18}$$

and

$$\hat{T}_{op}(k_z) = 1 - \sqrt{(1 - \frac{k_z^2}{k_0^2})}. \tag{3.19}$$

With these operators defined, the marching algorithm calculates the PE field function $\psi(r,z)$ from

$$\psi(r + \Delta r, z) = e^{-ik_0 \Delta r U_{op}(r,z)} \mathbf{F}\{e^{-ik_0 \Delta r \hat{T}_{op}(r,k_z)} [\mathbf{F}^{-1}(\psi(r,z))]\}, \tag{3.20}$$

where $\mathbf{F}$ and $\mathbf{F}^{-1}$ are the normal and inverse Fourier transform operators, respectively. This expression for the PE field function ψ is then inserted into Equations (3.13) and (3.1) to produce time-harmonic solutions to the PE field. For broadband signals, the SSF algorithm solves for the PE field for a set of discrete frequencies evenly spaced throughout the bandwidth of interest.

C. MONTEREY-MIAMI PARABOLIC EQUATION (MMPE) MODEL

The MMPE model (Smith, 1996) is a follow on to the University of Miami Parabolic Equation (UMPE) model (Smith and Tappert, 1993). This model is primarily a research model, and is widely used for acoustic propagation simulations at the Naval Postgraduate School. All modeling performed in this thesis was accomplished using the MMPE model, with slight variations described later. The following paragraphs describe the basic usage of the MMPE.

The MMPE is written in FORTRAN, and requires the presence of seven input files. The main input file, "pefiles.inp", defines the other six input files and determines such basic parameters as total range and depth, range step, and reference sound speed. The other six input files allow the user to input environmental data for the water column and two distinct bottom layers, as well as for source characteristics.

For the environmental data, the user can input the sound speed profile and the bottom bathymetry for the main water column, a sediment layer, and a deep layer. If only two layers are desired, the deep layer can be defined deeper than the maximum computational depth to exclude it from the model. The bathymetry can be as finely resolved as desired. Additionally, the user can input many other range dependent parameters, including sound speed, sound speed gradient, shear speed, shear attenuation, compressional attenuation, and density. The user supplied source data includes the center frequency, bandwidth, number of frequencies within the bandwidth, and the source depth.

The model allows for two types of sources, point sources or vertical line array sources.

The output of the MMPE model is a matrix of PE field function values, corresponding to the range/depth grid of interest for each discrete frequency. MATLAB files have been written (Smith, 1996) to process the data into desirable outputs. A full explanation of how to implement the MMPE model as well as a copy of the model itself can be downloaded from the World Wide Web at http://www.oalib.njit.edu/pe.html.

For the purpose of this thesis, the MMPE model had to be altered slightly. Specifically, provisions were made to incorporate phase conjugation of the signal when time reversal was desired. Additionally, a master MATLAB program was developed to control several runs of the model in succession, with data manipulations between each model run. The manipulations were required in order to simulate the reception and reflection/transmission of only a portion of the incoming signal. This allowed the simulation of submarine sized objects as targets and as sonar sources. For more detail on these variations to the MMPE, contact the author or the principal thesis advisor.

D. TIME ARRIVAL STRUCTURE

The results that are presented in the next chapter present the time arrival structure of the signal at some desired location. This section will present a brief

overview of how the MMPE calculates the time arrival structure of an acoustic field.

The MMPE model assumes that the transmitted signal is a single pulse $s(t)$ with spectral shape $S(f)$, centered at frequency f_0 with bandwidth BW. As mentioned in the previous section, the MMPE model calculates the PE field function ψ at each grid location for each of N discrete frequencies. The minimum and maximum frequencies used are calculated from f_0 and BW using

$$f_{\min} = f_c - \Delta f \frac{N}{2} \tag{3.21}$$

and

$$f_{\max} = f_c + \Delta f \frac{(N-1)}{2} \tag{3.22}$$

where

$$\Delta f = \frac{BW}{N-1}. \tag{3.23}$$

The time arrival structure for a given location requires the Fourier transform of the pressure field defined by Equation (3.13). Considering the whole pulse spectrum, Equation (3.13) can be rewritten as

$$p(r,z,f) = P_0 \sqrt{\frac{R_0}{r}} \psi(r,z,f) S(f) e^{ik_0 r} \tag{3.24}$$

with $k_0 = \frac{2\pi f}{c_0}$. By integrating over frequency, the time arrival structure can then be determined using

$$p(r,z,t) = P_0\sqrt{\frac{R_0}{r}}\int_{-\infty}^{\infty}\psi(r,z,f)S(f)e^{ik_0 r}e^{-i2\pi ft}df\,. \tag{3.25}$$

Since $k_0 = \frac{2\pi f}{c_0}$, the phase factor in the above equation becomes $e^{i2\pi f(\frac{r}{c_0}-t)}$.

Thus, the arrival time is expressed in reduced time, T, defined as

$$T = t - \frac{r}{c_0} \tag{3.26}$$

where t is the travel time of the pulse. Evaluating the full Fourier transform from $-f_{\max}$ to $+f_{\max}$ requires large transform sizes, which is extremely computationally intensive. So the MMPE model heterodynes the signal such that integration over only the bandwidth is required. Specifically,

$$\tilde{p}(r,z,T) = P_0\sqrt{\frac{R_0}{r}}\int_{-\frac{BW}{2}}^{\frac{BW}{2}}\psi(r,z,f'+f_c)S(f'+f_c)e^{-i2\pi f'T}df' \tag{3.27}$$

where $f' = f - f_c$ and $\tilde{p}(r,z,T) = p(r,z,t)e^{i2\pi f_c T}$. The addition of the phase factor in the above equation can easily be accounted for later. The time step involved is simply calculated from

$$\Delta T = T_{k+1} - T_k = \frac{1}{BW} \tag{3.28}$$

such that the duration of the time window is given by

$$T_{window} = (N-1)\Delta T = \frac{N-1}{BW}\,. \tag{3.29}$$

One final factor to consider is the choice of N, the number of discrete frequencies evaluated by the MMPE model. Since N is also the transform size it is computationally much more efficient to choose an N that is a power of two, which allows use of superior FFT algorithms. Additionally, since multipath propagation stretches the transmitted pulse in time, N must be large enough to prevent a wrap around effect. This wrap around effect is caused by a pulse elongation greater than the time window. Thus, N should be chosen sufficiently large to ensure the time window is long enough.

THIS PAGE INTENTIONALLY LEFT BLANK

IV. RESULTS

This chapter presents the results of six different model simulations run at various source-to-target ranges. These simulations were designed to study the applicability of time-reversal acoustics to active sonar. In general, active sonar is used to locate, localize, or track a target. In order to accomplish this, an acoustic signal is transmitted into the water, reflects off of the target, and returns to the original source. If the return signal strength is sufficiently high, such that it can be recognized above background noise, then a detection is made. Time-reversal acoustic methods could aid in this process by increasing the return signal strength. In the time-reversal method, the acoustic signal that reflects off of the target and returns to the source is received and reversed in time. For modeling purposes this time reversal is accomplished by phase conjugation in the frequency domain, as explained in Chapter II. This time-reversed signal is then amplified back up to the maximum amplitude of the original transmission, retransmitted, and reflected off of the target. Because of the focusing effect of time-reversal acoustics and the increased energy put into the water with the time-reversed transmission as described in Chapter II, this second signal returns with a significantly higher signal strength.

The simulations performed for this thesis consisted of two types. First, the source-to-target range was held constant and the apertures of both the target and receiver array were varied. Second, the apertures were fixed at a practical

size and the target was allowed to move between transmissions. The signal enhancement due to the time-reversal process was determined in each case by comparing the minimum pulse transmission loss of the time-reversed signal return to that of the original transmission.

A. MODEL SIMULATION DATA

The model simulations performed for this thesis all used the same environment. This environment was an isovelocity, flat bottom, range-independent ocean waveguide. Specific data for this environment is shown in Table 4.1. This environment was chosen for its simplicity; however, it should be noted that other more complicated environments have been demonstrated to possess the same TRA focusing properties as the simple environment used here (Abrantes, 1999).

Water sound speed	1500 m/s	Bottom shear speed	0.0
Bottom depth	100 m	Bottom shear attenuation	0.0
Bottom sound speed	1800 m/s	Center frequency	1000 Hz
Bottom density	2 g/cm^3	Bandwidth	500 Hz
Bottom compressional attenuation	0.0	# of frequencies	1024

Table 4.1

For each model simulation, a point source at a depth of 40m transmitted a pulse that propagated downrange to a target. The pulse transmitted had a center frequency of 1000 Hz with a 500 Hz bandwidth. This source data is also presented in Table 4.1. The target spanned the full water column for Run One, and was a 10m target centered at 40m depth for all subsequent runs. Upon reaching the target, the signal was reflected back to the source where it was received by some finite sized array. For Runs number One and Two, this array spanned the entire water column. Runs Three through Six used a 10m array centered at the original source depth of 40m. The signal received by this array was then time-reversed by phase conjugating the acoustic field function in the frequency domain. As discussed in Chapter II, the maximum amplitude of this time-reversed signal was increased to 0 dB to match the amplitude of the originally transmitted pulse. This signal was then transmitted by the array and reflected off the same target. For Runs One through Three the target remained at a fixed range from the source. For Runs Four, Five, and Six, the target moved closer by 500m, 1km, and 1.5km, respectively. These Runs are summarized in Table 4.2 below. The results of these simulations are shown in the following sections.

Run #	TRA array aperture	Target aperture	Target range&movement
1	Full water column	Full water column	Fixed at 5,10,and 15 km
2	Full water column	10m	Fixed at 5,10,and 15 km
3	10m	10m	Fixed at 5,10,and 15 km
4	10m	10m	Target closes 0.5 km
5	10m	10m	Target closes 1 km
6	10m	10m	Target closes 1.5 km

Table 4.2

B. CONSTANT RANGE, VARIABLE APERTURE SIMULATIONS

1. Full Water Column Target, Full Water Column TRA Array

The source pulse transmitted in Run One was reflected off of a full water column target at ranges of 5, 10, and 15 km. The return signal was received by a full water column array, time-reversed, adjusted to a maximum of 0 dB, and retransmitted. A comparison of the return signal strength from the original pulse and the time-reversed signal is shown in Figure 4.1 for a source to target range of 5 km.

It is interesting to note the multipath structure, which is evident in the upper panel of Figure 4.1 as well as following figures. A great deal of energy from the original pulse is manifested in these multipath structures between 6.65

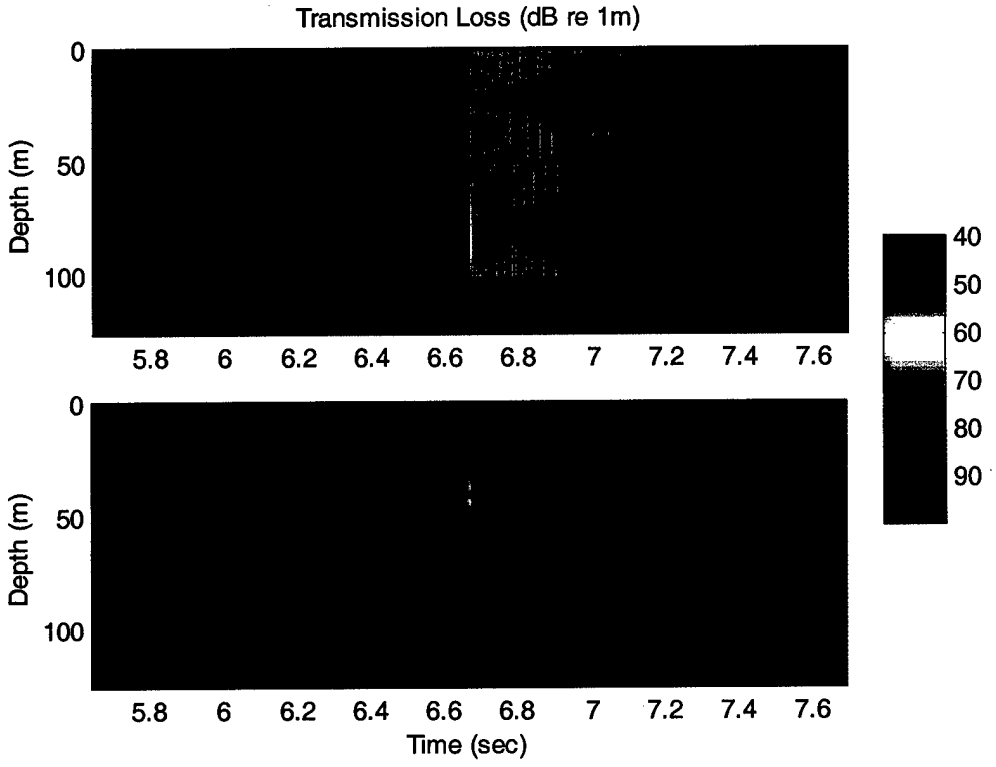

FIGURE 4.1: Run One, 5-km range. Upper panel is the return signal from the original pulse. Lower panel is the return from the time-reversed transmission.

and 7.6 seconds. In the lower panel of this figure, the multipath structure is mostly undone by the time-reversal process. A large portion of the energy that

had gone into the multipath structure from the original pulse has now focused at the original source depth in the TRA case.

The original signal arrived back at the source with a minimum pulse transmission loss (TL) of 66 dB re 1m. The time-reversed signal had a TL of 22 dB re 1m. This represents a signal level increase of 44 dB. As explained in Chapter II, this signal increase is a result of two factors. First, the time-reversed signal focuses the energy that was previously spread over time and depth to a small point, significantly increasing the returned signal strength. Second, more energy is transmitted in the time-reversed signal than in the original pulse because the signal is stretched out in time. The signal increase of 44 dB is artificially high due to the fact that the full column array can generate much more power than a point source could. This is taken into account in Figure 4.1 and all subsequent figures by limiting the instantaneous total power output of the array to that generated by a single point source. Initially, this was done by simply dividing the instantaneous total power of the array by the number of elements in the array. However, it was determined that this was a poor measure to use since certain elements contribute much more to the overall power of the array than others. Thus, a measure of "effective number of elements" was calculated by dividing the power transmitted from the element with the highest output by the total power output of the array. Then the instantaneous total power of the array was divided by this effective number of elements to simulate the instantaneous power output of a point source. For instance, if element i had the highest power

output in the array of N elements, the effective number of elements would be calculated by

$$\frac{1}{(eff\#elements)} = \frac{\int \psi_i^2}{\sum_N \int \psi^2}. \tag{4.1}$$

Note that the energy put into the water by the array is still much higher than that put in by the point source. This is due to the much longer pulse length of the TRA signal, and is one of the advantages of time-reversal acoustics. The adjusted TL for the time-reversed return is almost 40 dB re 1m. This is still an increase in signal strength of over 26 dB.

The comparison of returned signals for the 10-km case is shown in Figure 4.2. The original pulse reflected off of the target and returned with a minimum TL of 72 dB re 1m. The time-reversed signal returned with a TL of just over 29 dB re 1m. That is a signal increase of over 42 dB. After accounting for the extra power that the full column array could generate, the TL of the time-reversed signal was 47 dB re 1m, which is a signal increase of approximately 25 dB over the original return. For the remainder of this discussion, only the normalized value for the total power output of a point source will be stated. Both values will be presented in a summary table.

Also of note in the upper panel of Figure 4.2 is the apparent signal received around 12.4 seconds. This is the result of a wrap-around effect

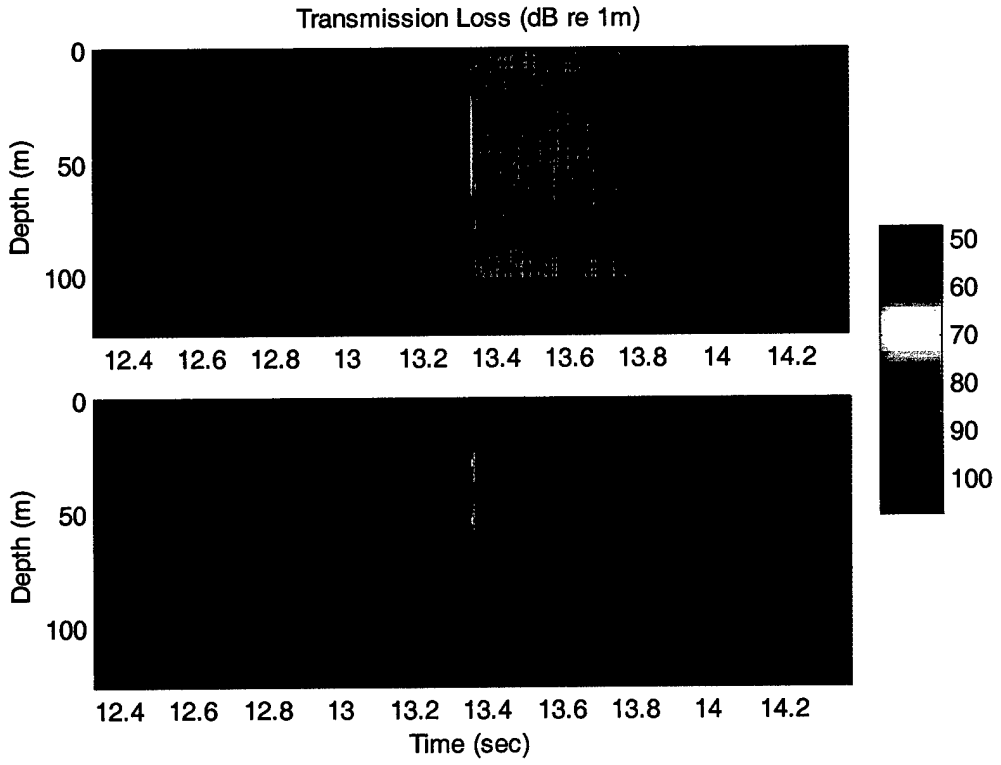

FIGURE 4.2: Run One, 10-km range. Upper panel is the return signal from the original pulse. Lower panel is the return from the time-reversed transmission.

experienced when converting between the frequency domain and the time domain. In later figures this wrap-around effect becomes more prominent; it does not affect the numerical results presented in this section at all.

Figure 4.3 compares the return signals for a range of 15 km. Here, the original pulse returned to the source with a TL of 75 dB re 1m, while the time-reversed signal had a TL of 47 dB re 1m. So the signal increase over the original

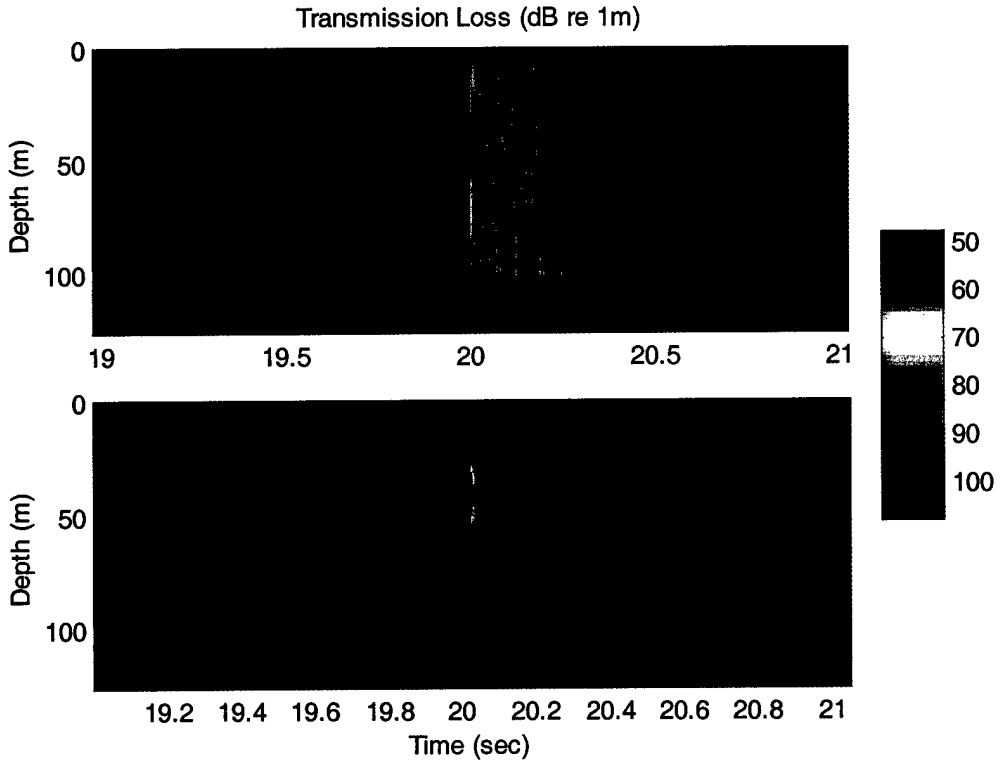

FIGURE 4.3: Run One, 15-km range. Upper panel is the return signal from the original pulse. Lower panel is the return from the time-reversed transmission.

pulse return was 28 dB. Also notice the focal region has lost some of its vertical tightness as the range has increased. This is because the higher modes are being more heavily attenuated at longer ranges due to boundary interactions.

2. 10m Target, Full Water Column TRA Array

The target aperture was reduced to 10m in Run Two. Again, the source pulse was reflected off of the target at ranges of 5, 10, and 15 km. Also as in

Run One, the return signal was received by a full water column array. After time-reversing the signal and adjusting the maximum amplitude to 0 dB, the signal was transmitted back toward the target. Figure 4.4 shows both the return from the original pulse and the return from the TRA signal for a source to target range of 5 km.

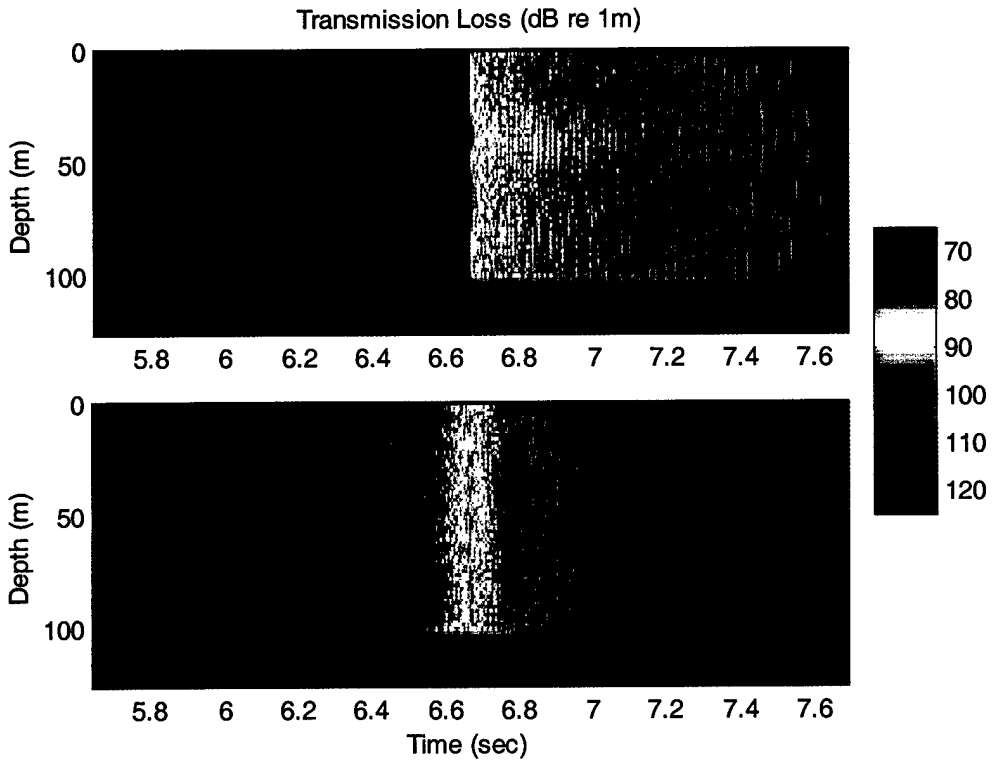

FIGURE 4.4: Run Two, 5-km range. Upper panel is the return signal from the original pulse. Lower panel is the return from the time-reversed transmission.

The minimum TL of the original pulse transmission was 77 dB re 1m. For the TRA signal, the minimum TL was 65 dB re 1m. This is still a signal enhancement of almost 12 dB. Also note the multipath structure in the upper panel of Figure 4.4. This structure is not as crisp as the structure shown in Figure 4.1 where the target spanned the entire water column. Additionally, the return from the time-reversed signal now contains significantly more sidelobe structure than it did in Figure 4.1. Since the target aperture was only 10m in Run Two (and all further Runs), only the portion of the multipath structure which interacts with the target is undone by the time-reversal process. The sidelobe structure that is seen in the lower panel of Figure 4.4 is the generally symmetric structure that is predicted in Chapter II.

The upper panel of Figure 4.4 also contains some sidelobe structure between 6.4 and 6.6 seconds. This is a result of the transformation of the signal from the frequency domain to the time domain. Because the target had a 10m aperture that did not taper off at the ends, the FFT that is performed to calculate the time-arrival structure produces sidelobes. This is a mathematical anomaly and is not a physical phenomenon.

The comparison of returned signals for the 10-km case is shown in Figure 4.5. The original pulse reflected off of the target and returned with a TL of almost 84 dB re 1m. The time-reversed signal returned with a TL of 70 dB re 1m, which is a signal increase of almost 14 dB over the original return.

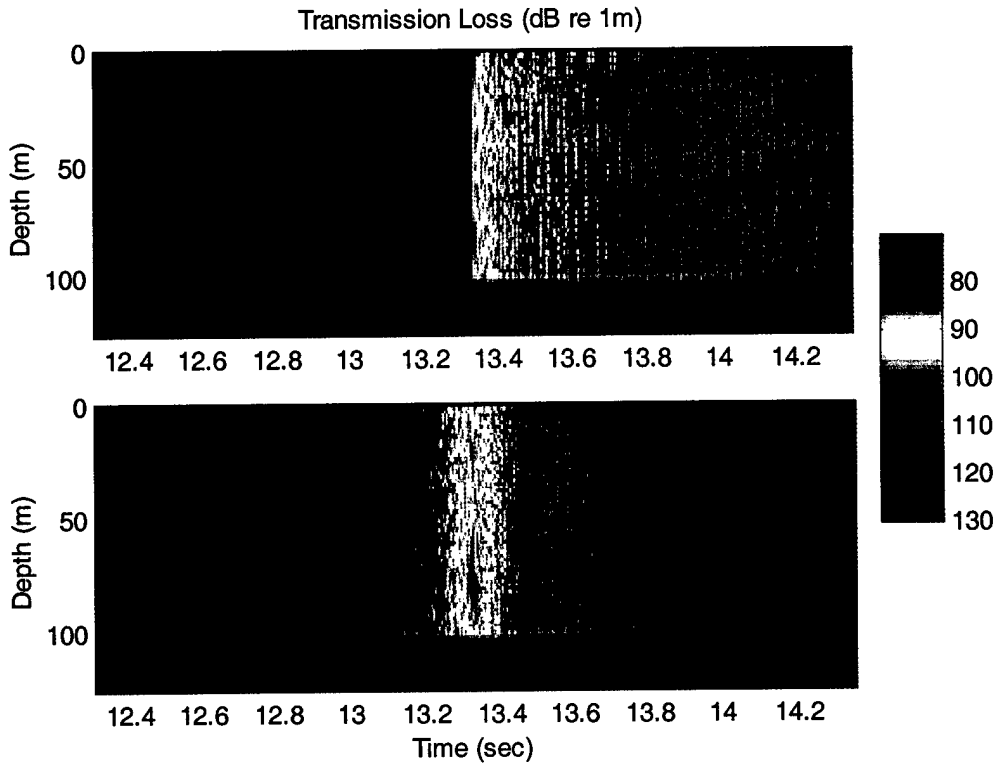

FIGURE 4.5: Run Two, 10-km range. Upper panel is the return signal from the original pulse. Lower panel is the return from the time-reversed transmission.

Figure 4.6 compares the return signals for a range of 15 km. Here, the original pulse returned to the source with a TL of 83 dB re 1m, while the time-reversed signal had a TL of 67 dB re 1m. So the signal increase over the original pulse return was almost 16 dB.

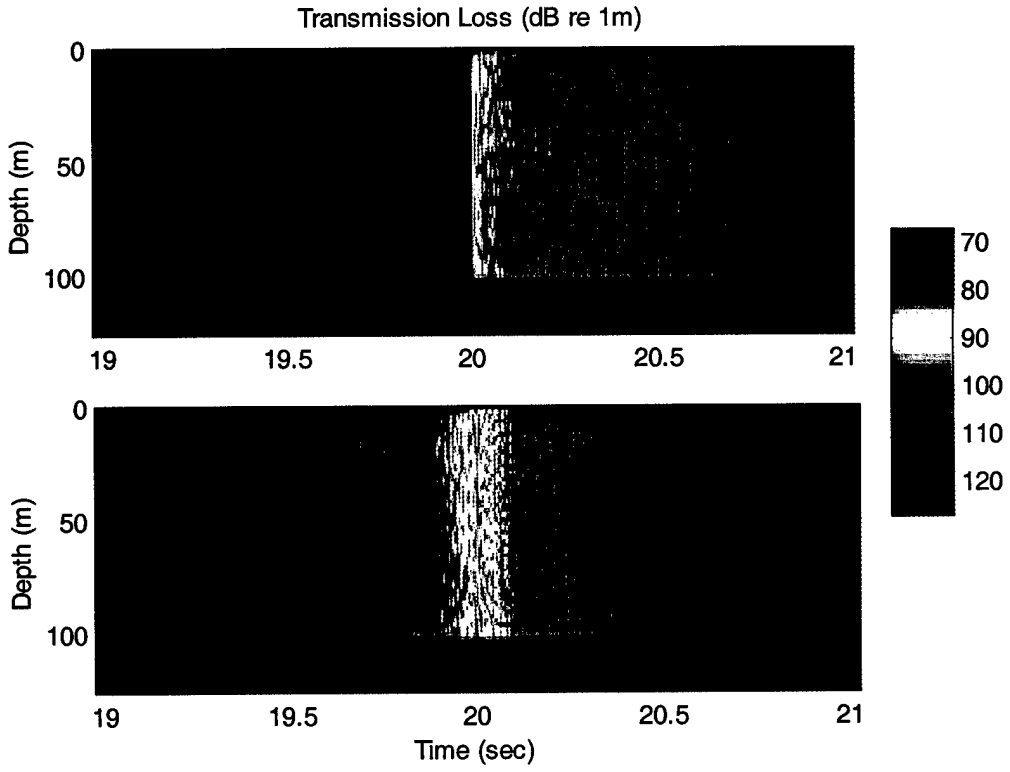

FIGURE 4.6: Run Two, 15-km range. Upper panel is the return signal from the original pulse. Lower panel is the return from the time-reversed transmission.

3. 10m Target, 10m TRA Array

In Run Three, the time-reversal array aperture was reduced to 10m, centered at the source depth of 40m. Thus, the source pulse reflected off of a 10m target and was received by the 10m TRA array. The received signal was time-reversed, adjusted to a maximum of 0 dB, and retransmitted. Again, the target remained at fixed distances of 5, 10, and 15 km. Run Three represents

the most realistic scenario so far for real world application. Modern submarine targets are on the order of 10m, and 10m arrays can reasonably be employed.

Figure 4.7 shows the return signal from the original pulse compared to the return from the TRA array transmission for the 5-km target range of Run Three.

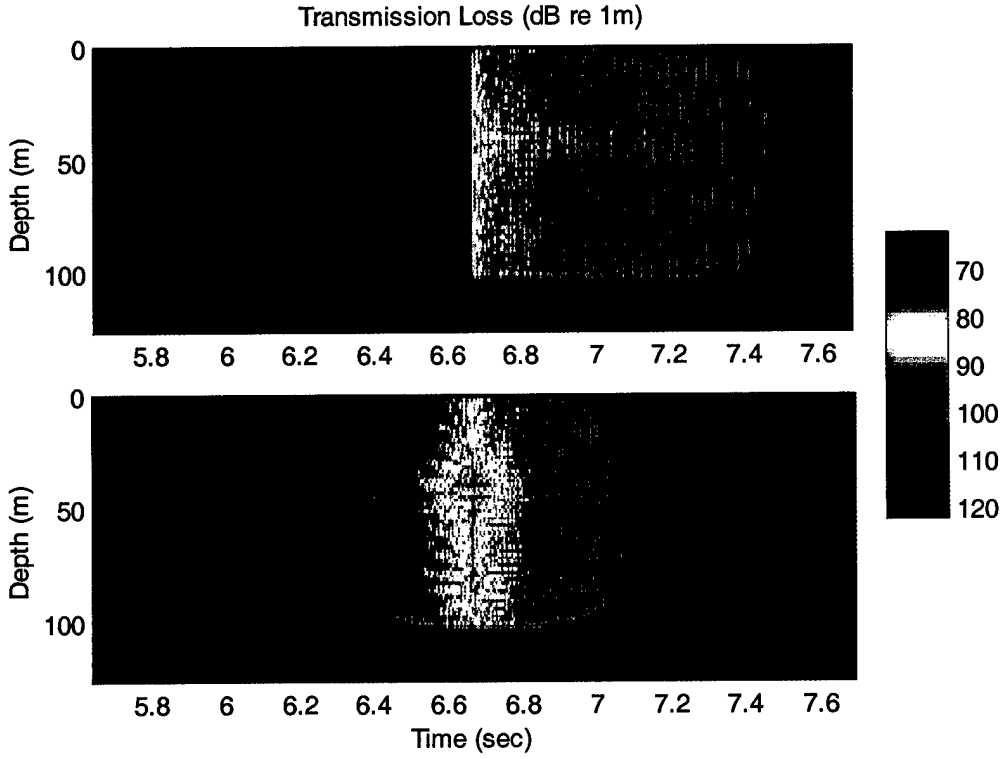

FIGURE 4.7: Run Three, 5-km range. Upper panel is the return signal from the original pulse. Lower panel is the return from the time-reversed transmission.

Note that the upper panel, showing the return from the original point source transmission, is exactly the same as the upper panel of Figure 4.4. The only difference between Run Two and Run Three is the aperture of the TRA array.

The return from the original pulse was again 77 dB re 1m, just as it was in Run Two. The return from the TRA transmission 62 dB re 1m. This is a very significant signal increase of 15 dB.

Figure 4.8 shows the comparison of original return to TRA return for the 10-km case. The return from the original pulse had a TL of 84 dB re 1m, just as it did in Run Two. The return from the TRA transmission was over 65 dB re 1m. This signal strength improvement of more than 18 dB is greater than the 15 dB

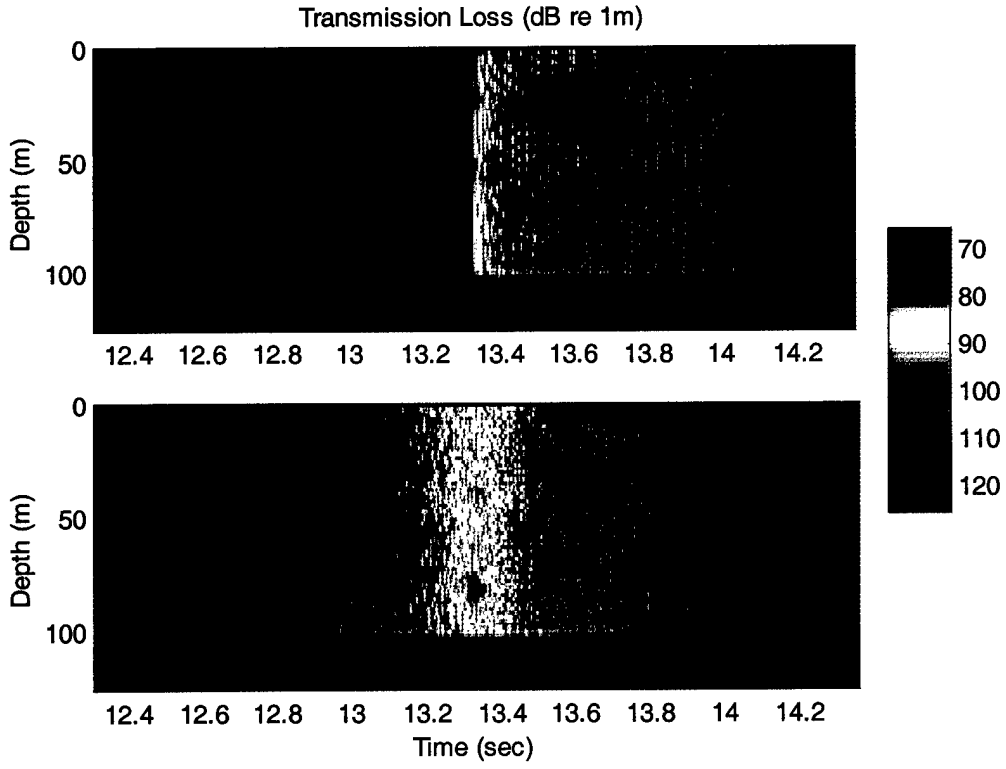

FIGURE 4.8: Run Three, 10-km range. Upper panel is the return signal from the original pulse. Lower panel is the return from the time-reversed transmission.

improvement seen in the 5-km case. This is due to the fact that at 5 km the modes have not fully separated, but by 10 km they have. With the modes fully separated more energy is put into each individual mode, and more focusing is achieved at the target.

It is interesting to notice that the return signal focuses at the source depth of 40m and also at a deeper depth of about 83m. The TL at the 83m depth is actually lower than that at the source depth by just over 2 dB. This second focus occurs only for the 10-km simulations and is a phenomenon that would probably not occur in more general, depth-dependent environments.

The 15-km case is shown in Figure 4.9. Here, the original pulse return had a

TL of 83 dB re 1m, while the TRA return had a TL of 67 dB re 1m, for a signal enhancement of 16 dB. This is also greater than the enhancement seen in the 5-km case because the modes have fully separated. However, it is less than the enhancement from the 10-km case, where the modes were also fully separated, because of attenuation of the higher order modes. Table 4.3 summarizes the results of Runs One through Three. Note that the TRA signal return becomes less clearly focused both vertically and temporally as the range to target is increased and as the aperture size is reduced.

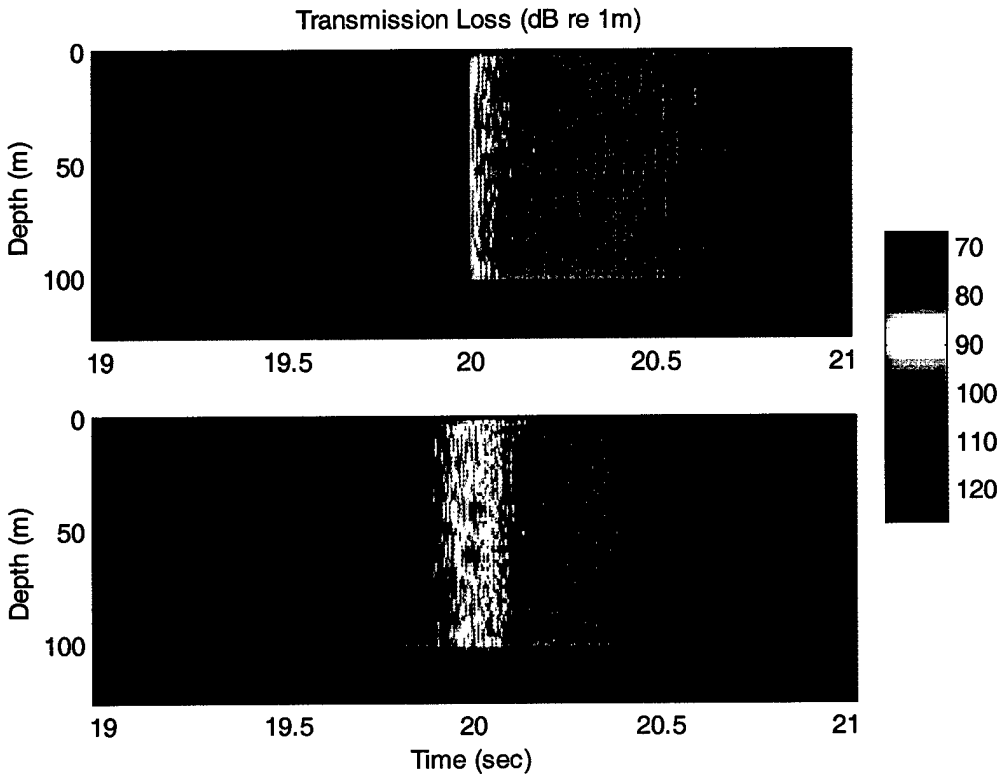

FIGURE 4.9: Run Three, 15-km range. Upper panel is the return signal from the original pulse. Lower panel is the return from the time-reversed transmission.

Run #	Source-target range	Original min pulse TL (re 1m)	TRA min pulse TL (re 1m)	Signal Enhancement	
				Total	Normalized
1	5 km	66 dB	40 dB	44 dB	26 dB
1	10 km	72 dB	47 dB	42 dB	25 dB
1	15 km	75 dB	47 dB	45 dB	28 dB
2	5 km	77 dB	65 dB	34 dB	12 dB
2	10 km	84 dB	70 dB	36 dB	14 dB
2	15 km	83 dB	67 dB	36 dB	16 dB
3	5 km	77 dB	62 dB	29 dB	15 dB
3	10 km	84 dB	65 dB	33 dB	19 dB
3	15 km	83 dB	67 dB	29 dB	16 dB

Table 4.3

C. CONSTANT APERTURE, VARIABLE RANGE SIMULATIONS

Runs One, Two, and Three compared the signal return from a point source transmission to the signal return from a TRA array transmission with fixed source-to-target ranges. The effects of changing target aperture and TRA array aperture were explored. Fixed source-to-target ranges are of practical interest since submarines operating in shallow water do not move at high speeds, and a likely target is a slow moving diesel submarine. However, it is important to realize that the range will not remain exactly constant. Therefore, the effect of a change in source-to-target range was explored in Runs Four, Five, and Six. These three Runs followed the same general method of Run Three, with one exception. After the original pulse reflected off the target and was received by the TRA array, the target moved closer before the TRA signal transmission. Target movements of 500 m, 1 km, and 1.5 km were simulated in the three Runs. All other parameters remained the same as those in Run Three.

1. 5 km Initial Target Range

The signal return from the original point source transmission for a 5-km range has already been shown in Runs Two and Three. This signal had a TL of 77 dB re 1m at the receiving aperture. The signal return from the TRA transmission for the 5-km range had a TL of 62 dB re1m. Figure 4.10 shows this TRA signal return in the upper panel. In three separate simulations, the target

was moved closer by ranges of 500m, 1 km, and 1.5 km. The signal return of the TRA transmission for each of these simulations is shown in the second, third, and fourth panels, respectively, of Figure 4.10.

When the target moved 500m closer to a range of 4.5 km, the return signal TL was 72 dB re 1m, for a signal enhancement of almost 5 dB over

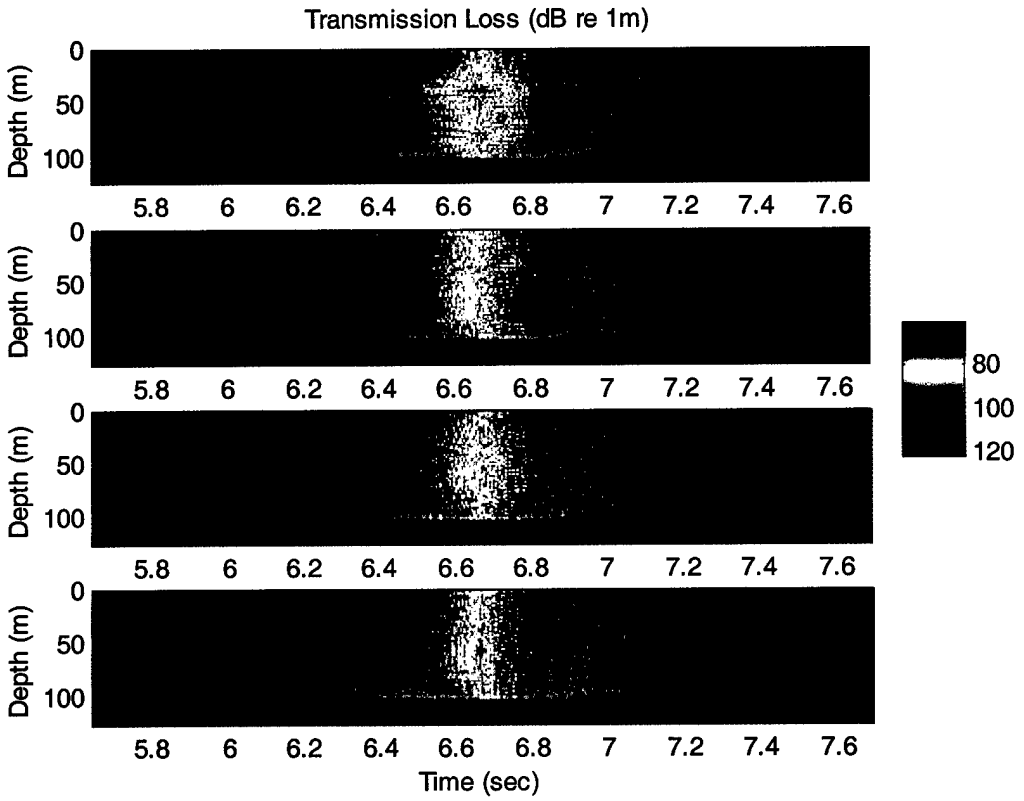

FIGURE 4.10: 5-km range. Upper panel is the return signal from the TRA transmission with a stationary target. Second, Third, and Fourth panels are the return from the time-reversed transmission after target range decreased by 500m, 1 km, and 1.5 km, respectively.

the original return of 77 dB re 1m. This is much lower than the 15 dB enhancement realized when the target did not move between transmissions, but it is still a significant increase. For the case where the target moved closer 1 km, the return signal TL was 74 dB re 1m. This yields a signal enhancement of just under 3 dB. Finally, when the target range decreased by 1.5 km the signal return was 69 dB re 1m, which is an improvement in signal strength of over 7 dB. This is larger than the improvement seen when the target moved shorter distances. This is due to the sidelobe property of the TRA focus. With a movement of 1.5 km, the target had shifted to a position with a higher sidelobe level.

2. 10 km Initial Target Range

The signal return from the original point source transmission for a 10-km range has also already been shown in Runs Two and Three. This signal had a TL of 84 dB re 1m at the receiving aperture. The return from the TRA transmission for this range had a TL of 65 dB re 1m. Figure 4.11 shows this TRA signal return in the upper panel. The target again was moved closer by ranges of 500m, 1 km, and 1.5 km in three simulations. The signal return of the TRA transmission for each of these simulations is shown in the second, third, and fourth panels, respectively, of Figure 4.11.

When the target moved 500m closer, to a range of 9.5 km, the return signal TL was 76 dB re 1m. This represents a signal enhancement of 8 dB.

Again, this signal increase is much lower than the 18 dB enhancement realized when the target did not move between transmissions, but it is still a significant increase. For the case where the target moved closer 1 km, the return signal TL was 78 dB re 1m, giving a signal enhancement of just under 6 dB.

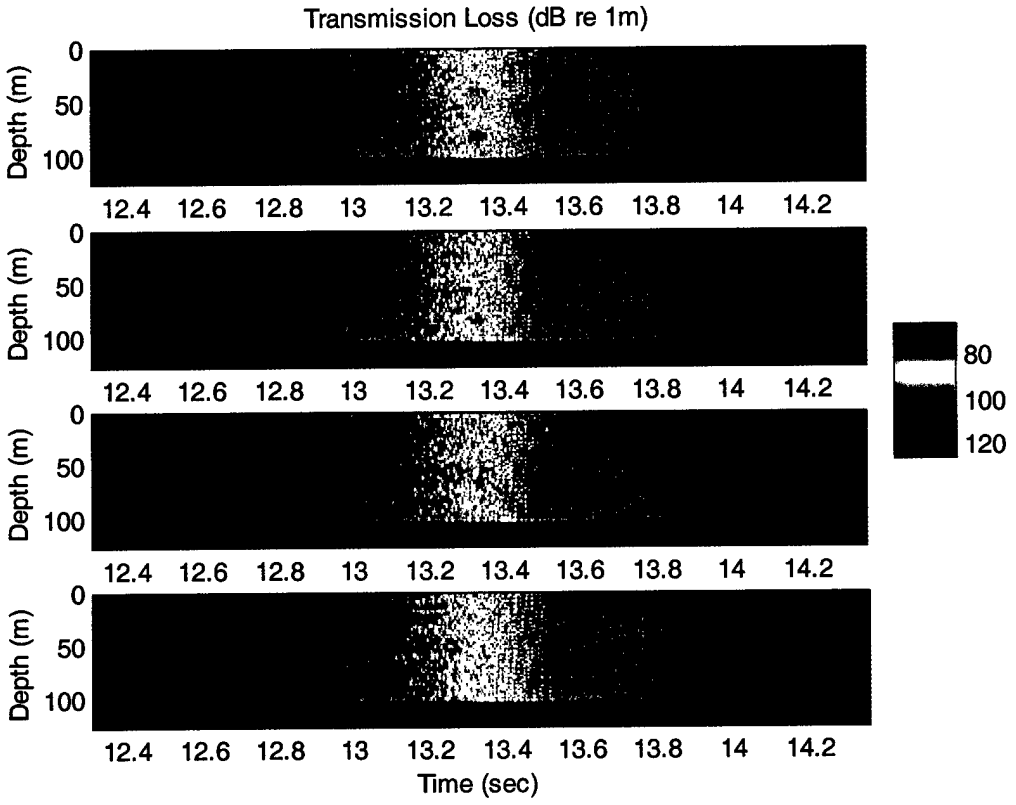

FIGURE 4.11: 10-km range. Upper panel is the return signal from the TRA transmission with a stationary target. Second, Third, and Fourth panels are the return from the time reversed transmission after target range decreased by 500m, 1 km, and 1.5 km, respectively.

Finally, when the target range decreased by 1.5 km the signal return was 79 dB re 1m, which is an improvement in signal strength of 5 dB. Thus, the power-adjusted signal enhancement drops significantly when the target range changes between transmissions, but the drop is not radically different for a relatively wide spread of range changes.

3. 15 km Initial Target Range

For the final source-to-target range considered, 15 km, the signal return from the TRA transmission with a stationary target is shown in the upper panel of Figure 4.12. This is the same signal return that was shown in Runs Two and Three. This signal had a TL of 83 dB re 1m at the receiving aperture. The signal return from the TRA transmission was 67 dB re 1m. Once again, the target was moved closer by ranges of 500m, 1 km, and 1.5 km. The signal return of the TRA transmission for each of these simulations is shown in the second, third, and fourth panels, respectively, of Figure 4.12.

For this case, the movement of the target 500m closer is the smallest percentage range change considered in this thesis. When the target moved 500m closer the return signal TL was 75 dB re 1m, for a signal enhancement of almost 8 dB. Again, this is much lower than the 16 dB enhancement realized when the target did not move between transmissions, but it is still a significant increase. For the case where the target moved closer 1 km the return signal TL

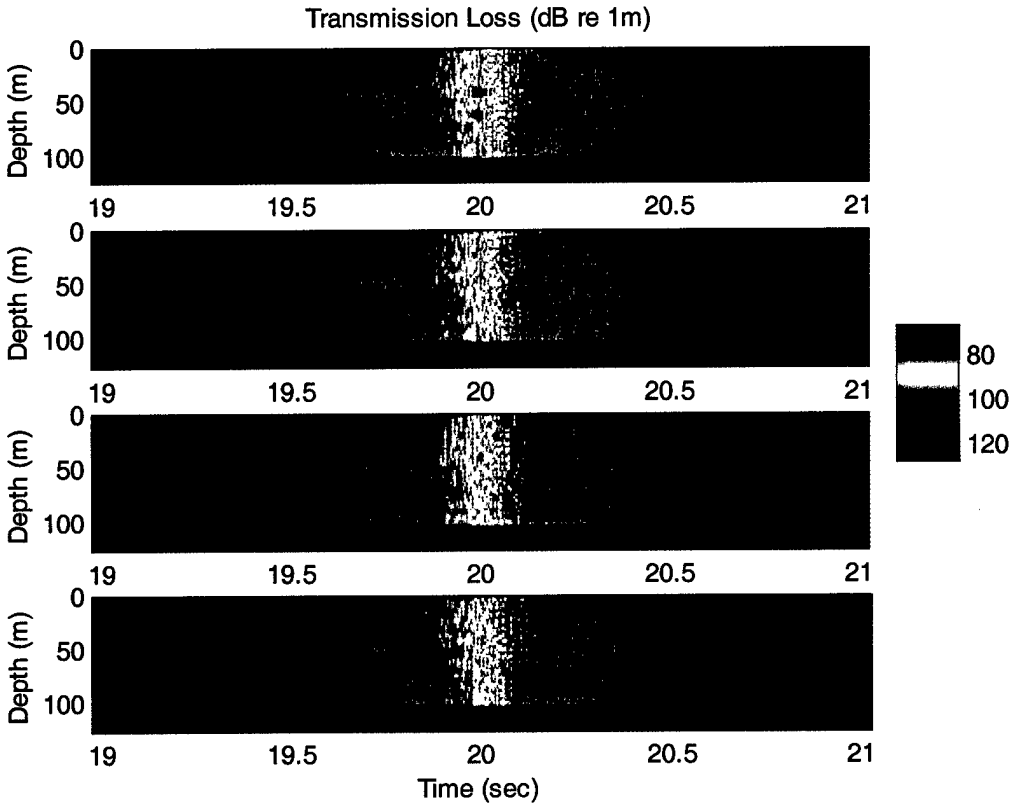

FIGURE 4.12: 15-km range. Upper panel is the return signal from the TRA transmission with a stationary target. Second, Third, and Fourth panels are the return from the time reversed transmission after target range decreased by 500m, 1 km, and 1.5 km, respectively.

was 78 dB re 1m, giving a signal enhancement of just under 5 dB. Finally, when the target range decreased by 1.5 km, the signal return was 77 dB re 1m, which is an improvement in signal strength of 6 dB. This enhancement is larger than that seen when the target moved 1 km, but less than the improvement when the

target moved only 500m. Again, this variability of signal enhancement with different target range movements can be attributed to the sidelobe structure of the TRA focus. The results of Runs Four through Six are summarized in Table 4.4.

Initial source-target range	Range change	Original min pulse TL (re 1m)	Min TRA pulse TL (re 1m) after movement	Signal Enhancement	
				Total	Normalized
5 km	.5 km	77 dB	72 dB	19 dB	5 dB
5 km	1 km	77 dB	74 dB	17 dB	3 dB
5 km	1.5 km	77 dB	69 dB	21 dB	8 dB
10 km	.5 km	84dB	76 dB	22 dB	8 dB
10 km	1 km	84 dB	78 dB	21 dB	6 dB
10 km	1.5 km	84 dB	79 dB	19 dB	5 dB
15 km	.5 km	83 dB	75 dB	21 dB	8 dB
15 km	1 km	83 dB	78 dB	18 dB	5 dB
15 km	1.5 km	83 dB	77 dB	19 dB	6 dB

Table 4.4

THIS PAGE INTENTIONALLY LEFT BLANK

V. CONCLUSIONS

The modeling performed in this thesis compared the signal strength of an active sonar return using TRA methods to the strength of the return from a single pulse. In the first set of simulations the range between source and target remained fixed at either 5, 10, or 15 km, while the apertures of the target and TRA array were varied.

In the first of these fixed range runs, the target and the TRA array spanned the entire water column. The resulting temporal focusing from the TRA array provided a signal enhancement of over 26 dB for the 5-km case. This best case enhancement is testament to the fact that time-reversal acoustics does indeed work, and it stands as a reference point for further comparisons. With the same target and TRA array, the range was increased to 10 km and then 15 km. For these cases the signal enhancement was 25 dB and 28 dB, respectively. Range does not appear to play a dominant role in determining the signal enhancement due to time-reversal acoustics. This is due to the simplistic environment with no bottom loss used in the modeling. The signal enhancement would normally be expected to degrade at longer ranges due to attenuation of higher modes.

When the target was reduced to a 10-m target and the TRA still spanned the entire water column, the signal enhancement for the 5-km case was reduced to 12 dB. The signal enhancements for the 10-km and 15-km cases were 14 dB

and 16 dB, respectively. This data suggests that target aperture is very important in determining the amount of signal enhancement TRA can provide. Again, the difference in enhancement between the ranges is not particularly significant for this environment.

In the last of the fixed range runs, both the target and the TRA array had apertures of 10 m. The signal enhancements for the 5, 10, and 15-km cases were 15 dB, 18 dB, and 16 dB, respectively. Once again the data support the conclusion that range is not the determining factor in TRA signal enhancement. The most interesting point about the data, however, is that the signal enhancement for this case is actually slightly better than the enhancement realized when the TRA array spanned the entire water column. Note that this data is adjusted to account for the excess power generated in the array as compared to a point source, as described in Chapter IV. The fact that the signal enhancement is greater for the 10 m TRA array can be explained by realizing that the portion of the water column that was sampled contained a lower average energy than the average energy contained in the entire water column. Thus, the boosting of intensity up to 0 dB for the time-reversed signal added more to the limited aperture TRA array than the full water column array.

The second set of simulations run for this thesis held the apertures of both the target and TRA array fixed at 10 m and varied the range of the target between transmissions. The initial range of the target was again 5, 10, and 15

km. This time, however, the target moved closer to the source by 500 m, 1 km, or 1.5 km between the initial reflection and the TRA array transmission.

For the case where the target was initially at a range of 5 km, the signal enhancement found in the fixed range case was 15 dB. When the target moved 500 m closer between transmissions, the enhancement decreased to only 5 dB. This is a drastic reduction; however, a 5 dB enhancement is still a significant signal improvement. When the target moved by 1 km the enhancement was 3 dB, while for a target movement of 1.5 km the enhancement was 7 dB. It is interesting to note that the enhancement was greatest when the target moved the most. The large drop from the stationary target case suggests that the TRA focus in range is very sharp. The fact that enhancement was greater for the largest movement is consistent with the fact that the TRA focus has sidelobes.

When the target was initially at 10 km, the fixed range enhancement was 18 dB. Again, there was a significant drop in signal enhancement when the target moved between transmissions. For target movements of 500 m, 1 km, and 1.5km, the signal enhancements were 8 dB, 6 dB, and 5 dB, respectively. While these enhancements are much lower than the fixed range enhancement of 18 dB, they are still significant signal improvements.

Finally, when the target was at an initial range of 15 km, the fixed range enhancement was 16 dB. The signal enhancements for target movements of 500 m, 1 km, and 1.5 km were 8 dB, 5 dB, and 6 dB, respectively. The 500 m

target movement represented just 3.3% of the range between source and target, the smallest percentage change studied in this thesis. The 8 dB drop in signal enhancement for that case further supports the conclusion that the TRA focus is very narrow in range.

The signal enhancement for the fixed source-to-target cases did not change drastically for the different ranges examined. It is interesting to note, however, that the return signal level for these cases was lowest for the 5 km case, but was higher for the 10 km case than for the 15 km case. One possible explanation for this is that the modes are not fully separated at a range of 5 km, but they are by 10 km. However, the higher modes are attenuated more severely by the 15-km range.

Another important feature to draw out of the data is the presence of sidelobes, which are predicted by the theory developed in Chapter II. These sidelobes have a significant effect on the signal enhancement when the source-to-target range changes between transmissions.

The use of a TRA array provides a dramatic increase in return signal strength. This is especially true when the source-to-target range is fixed, but is also true when this range changes between transmissions. Since the range would not change radically in the time between transmissions in a real world scenario, a TRA sonar system may provide a significant advantage. The modeling in this thesis demonstrated that signal enhancements on the order of

15 dB for the fixed range case, and 5 dB for a moving source/target case can be expected for this simplistic type of environment.

Further study is needed to determine how sensitive the TRA signal enhancement is to more realistic environments, range changes, and different source characteristics such as frequency and bandwidth. Another area that deserves further study is the examination of the properties of the sidelobes generated by the TRA transmission. It has been shown in this thesis that continued research into time-reversal acoustics is warranted, and could ultimately lead to the development of a practical active TRA sonar system.

THIS PAGE INTENTIONALLY LEFT BLANK

LIST OF REFERENCES

Abrantes, A. M. A., Smith, K. B., and Larraza, A., (**1999**) "Examination of time-reversal acoustics and applications to underwater communications," *Journal of the Acoustical Society of America*, Vol. 105, pp. 1364.

Chin-Bing, S.A., King, D.B., Davis, J.A., and Evans, R.B., (**1993**) "Lloyd's Mirror – Wide Angle Propagation," *PE Workshop II: Proceedings of the Second Parabolic Equation Workshop*, Naval Research Laboratory NRL/BE/7181-93-0001 (US Government Printing Office, pp. 62-67).

Hardin, R.H. and Tappert, F.D., (**1973**) "Applications of the split-step Fourier method to the numerical solution of nonlinear and variable coefficient wave equations," *SIAM Rev. 15, pp. 423.*

Jensen, F.B., Kuperman, W.A., Porter, M.B., and Schmidt, H., (**1994**) *Computational Ocean Acoustics*, American Institute of Physics Press, Woodbury, NY.

Kuperman, W.A., Hodgkiss, W.S., Song, H.C., Akal, T., Ferla, C., and Jackson, D.R. (**1998**) "Phase conjugation in the ocean: Experimental demonstration of an acoustic time-reversal mirror," *Journal of the Acoustical Society of America*, Vol. 103, pp. 25-40.

Smith, K. B., Abrantes, A. M. A., and Larraza, A., (**2000**) "Examination of time-reversal acoustics in shallow water and applications to non-coherent underwater communications," *Journal of the Acoustical Society of America* (submitted).

Smith, K.B. and Tappert F.D., (**1994**) "UMPE: The University of Miami Parabolic Equation Model, *Version 1.1,"* MPL Technical Memorandum 432, 1993 (revised September 1994).

Tappert, F.D., (**1974**) "Parabolic equation method in underwater acoustics," *Journal of the Acoustical Society of America Suppl. 1,* Vol. 55, S34.

Thomson, D.J. and Chapman, N.R., (**1983**) "A wide-angle split-step algorithm for the parabolic equation," *Journal of the Acoustical Society of America,* Vol. 74, pp. 1848-1854.

THIS PAGE INTENTIONALLY LEFT BLANK

INITIAL DISTRIBUTION LIST

1. Defense Technical Information Center 2
   8725 John J. Kingman Rd. STE 0944
   Ft. Belvoir, VA 22060-6218

2. Dudley Knox Library 2
   Naval Postgraduate School
   411 Dyer Rd.
   Monterey, CA 93943-5101

3. Mr. Ken Dial 1
   Code 321SS
   Office of Naval Research
   800 N. Quincy St. Ballston Tower 1
   Arlington, VA 22217-5660

4. Dr. John Tague 1
   Code 321US
   Office of Naval Research
   800 N. Quincy St. Ballston Tower 1
   Arlington, VA 22217-5660

5. Professor Kevin B. Smith 5
   Code PH/Sk
   Physics Department
   Naval Postgraduate School
   Monterey, CA 93943-5117

6. CDR Mitch Shipley, USN 2
   Code PH/Sm
   Physics Department
   Naval Postgraduate School
   Monterey, CA 93943-5117

7. LT Thomas A. Winter, USN 2
   366A Tullibee Ave.
   Groton, CT 06340